In vivo imaging of endocrine islets of Langerhans in mice with extended focus Optical Coherence Microscopy

Author list:

M. Villiger[1], J. Goulley[2], M. Friedrich[1], A. Grapin-Botton[2], P. Meda[3], T. Lasser[1], and R. A. Leitgeb[1,4]

Affiliations:

[1]Laboratoire d'Optique Biomédicale, Ecole Polytechnique Fédérale de Lausanne, Station 17, CH-1015 Lausanne

[2]Swiss Institute for Experimental Cancer Research (ISREC)/ Ecole Polytechnique Fédérale de Lausanne, Ch. des Boveresses 155, CH-1066 Epalinges

[3]Department of Cell Physiology and Metabolism, University of Geneva, Medical School, CMU, Rue Michel Servet 1, CH-1211 Geneve 4

[4]Center of Biomedical Engineering and Physics, Medical University of Vienna, Waehringerstrasse 13, A-1090 Vienna

Corresponding author:

MartinVilliger
EPFL STI IMT LOB
BM 5140 (Bâtiment BM)
Station 17
CH-1015 Lausanne
Switzerland
Phone: +41 (0)21 693 77 73
Fax: +41 (0)21 693 78 20
martin.villiger@epfl.ch

Word count abstract: 230

Word count main text: 3961

Number of figures: 6

Full text and supplementary material are available at: http://www.springerlink.com/content/nl47001u2700lk34/

Aims – Structural and functional imaging of the islets of Langerhans and the insulin-secreting beta cells represents a significant challenge and a long lasting objective in diabetes research. *In vivo* microscopy offers valuable insight into beta cell function but entails severe limitations regarding sample labelling, imaging speed and depth, and was primarily performed on isolated islets lacking native innervations and vascularisation. This article introduces extended focus optical coherence microscopy (xfOCM) to image murine pancreatic islets in their natural environment *in situ*, i.e. *in vivo* and in a label free condition.

Methods – Ex vivo measurements on excised pancreata were performed and validated by standard immunohistochemistry to investigate the structures which can be observed with xfOCM. The influence of streptozotocin on the signature of the islets was investigated in a second step. Finally, xfOCM was applied to measurements of the murine pancreas *in situ* and *in vivo*.

Results – xfOCM circumvents the fundamental physical limit that trades lateral resolution for depth of field, and achieves fast volumetric imaging with high resolution in all three dimensions. It allows label-free visualisation of pancreatic lobules, ducts, blood vessels and individual islets of Langerhans *ex vivo* and *in vivo*, and detects streptozotocin-induced islet destruction.

Conclusions – Our results demonstrate the potential of xfOCM in diabetes research for high resolution animal *in vivo* studies assessing islet structure and function, and aiming towards longitudinal studies of diabetes progression and islet transplants.

Keywords

Mouse, Islets, Imaging

Abbreviations:

MRI	Magnetic Resonance Imaging
NA	Numerical Aperture
OPT	Optical Projection Tomography
OCM	Optical Coherence Microscopy
OCT	Optical Coherence Tomography
PET	Positron Emission Tomography
xfOCM	extended focus Optical Coherence Microscopy

It is essential to be able to measure the structure and function of individual islets of Langerhans [1]. To further the understanding of diabetes' mechanisms and to evaluate treatments of the disease, monitoring of functional islet parameters is mandatory. Most applicable to a clinical setting are positron emission tomography (PET) and magnetic resonance imaging (MRI) [2, 3, 4]. Their medical potential is undoubted, but to date, only optical methods have provided the necessary spatial resolution to resolve individual islets [5]. Although most of these methods are likely to have little impact in the clinical practice and

human *in vivo* imaging, they are indispensable and complementary tools to provide insight into the cellular and molecular mechanisms of this disease.

The preparation of sections with immunocytochemical labelling is the standard method to visualise sub-cellular structures and to discriminate between the various islet cell types. This method is time consuming and only gives a two dimensional view of the tissue slices. Optical projection tomography (OPT) [6] has been used to image the adult mouse pancreas and to retrieve the three dimensional and undistorted structure of the tissue, which may be quantified. However, such approaches require sample fixation and immunolabelling, and hence, cannot be applied *in vivo* [7, 8].

Likewise, functional studies are performed *in vitro* on isolated islets [9, 10] and often after fluorochrome labelling, which is prone to bleaching and phototoxicity. Two-photon microscopy reduces these effects [11]. Even so, the islets are deprived of their natural tissue environment which limits the physiological relevance of such studies.

In recent work [12] islets have been transplanted into the mouse eye. Engrafted on the iris they could be repeatedly imaged using the eye as a natural body window. This minimally invasive approach allows longitudinal monitoring of individual islets, visualisation of islet vascularisation, beta cell function and death, by using two-photon fluorescence microscopy in combination with appropriate fluorochromes and transgenic mouse models expressing green fluorescent protein.

Here we report on the first three dimensional *in vivo* imaging of the murine pancreas macro- and microstructure by an approach that requires no labelling and that works *in situ*. The islets are studied in their natural environment with their native innervation and vascularisation. The technique we have developed is extended focus Fourier domain optical coherence microscopy (xfOCM) [13]. It is based on optical coherence tomography (OCT), an emerging biomedical imaging modality that provides cross-sectional views of the subsurface microstructure of biological tissue [14, 15]. It employs light from a low coherence source that is back-scattered by differences in the tissue refractive index and that is combined with a strong reference signal. The detection in the Fourier, or frequency, domain spectrally separates the interference signal into its chromatic components and records the resulting pattern with a line camera. Processing of this pattern extracts the sample structure along the axial direction in parallel without axial scanning and with a high resolution of 2-3μm [16]. Together with its high sensitivity [17] that allows imaging several hundred micrometers into the tissue, Fourier domain OCT provides an exceptional speed advantage over other optical imaging methods, making it a confirmed tool for comprehensive volumetric imaging [18, 19].

Classical optical coherence microscopy (OCM) [20, 21] uses standard focusing optics to obtain high lateral resolution. The resulting short depth of field hampers Fourier domain OCT's parallel depth extraction and necessitates time-consuming scanning in all three dimensions which makes *in vivo* measurements difficult. Our novel approach has been to circumvent this compromise between lateral resolution and depth of field by engineering an extended focus that is scanned rapidly in the lateral directions.

Our study validates this approach for the *in vitro* and *in vivo* imaging of islets of Langerhans and evidences its potential for structural and functional studies.

RESEARCH DESIGN AND METHODS

xfOCM Setup. The prototype xfOCM system developed for this study provides a high, near isotropic resolution of 1.3 μm in the lateral and 2 μm in the axial direction, revealing structural details and fine cell arrangements over an axial range of 300 μm. The basic layout is displayed in fig. 1. The linearly polarized light source (Ti:Sapphire laser, Femtolasers, Vienna, Austria; central wavelength: 780 nm; spectral full width at half maximum: 130nm) is collimated (L_S: f = 8.2 mm) and split by the beamsplitter BS_1 into sample and reference arm (Fig. 1). The sample beam passes through the axicon (apex angle 180°-2β =175°) and is relayed (L_R: f = 100 mm) through the scanning system, which provides rapid lateral scanning. The two galvo scanners rotate the beam around a common pivot point and the lens L_T (f = 164 mm) creates finally a thin annulus of diameter $d \approx f\beta(n-1)$ in the back aperture of the objective (Zeiss Neofluar, 10x, NA 0.3). The scanning system's common pivot point, in a conjugate plane of the objective's back aperture, is crucial to the correct scanning of the beam in the lateral directions. In the sample region, the different contributions converge in the proximity of the focal plane and interfere to create a Bessel-like illumination pattern in the radial direction, propagating nearly diffraction-free over a long axial distance of nearly 400 μm with a uniform lateral definition of ~1.3 μm (see small inlet in fig. 1). The light back-scattered from the sample is decoupled from the illumination path by beamsplitter BS_2 to prevent a double pass through the axicon. The descanned signal is combined with the reference beam and coupled into the detection fibre of NA 0.12.

This detection scheme has a twofold impact. First, the signal is detected with high efficiency, resulting in sufficient sensitivity to image biological samples. Second, with the detection aperture smaller than the annulus diameter, light from specular reflection is suppressed, producing a dark field effect. Nevertheless, the resulting detection volume acts as apodisation on the illumination needle, producing an effective extended focus of ~300 μm.

The signal is analysed with a spectrometer consisting of a transmission grating (1200 lines/mm) and a linear camera with 2048 pixels (Atmel Aviva) set to an integration time of 40 μs, working at a 20 kHz depth profile rate. The illumination power on the sample was 3-4 mW. Adjacent scanning points were separated by between 0.2 and 2.5 μm, varying the area of one scan between 100 x 200 μm and 2 x 1.2 mm.

Signal processing. The signal recorded on the spectrometer can be expressed as $I(k) = |A_r|^2 + \alpha^2|A_s|^2 + 2\mathrm{Re}\{ A_r A_s^* \int h(z) e^{i2k(z-z0)} dz \}$, where A_r and A_s are the electromagnetic field amplitudes in the reference and sample arm respectively, h(z) represents the local reflectivity of the sample structure as a function of z, $k = 2\pi/\lambda$ is the wavenumber, and $\alpha^2 = |\int h(z) e^{i2k(z-z0)} dz|^2$ is the total reflectivity of the sample. To reconstruct the sample structure, we compute the Fourier Transform of the signal after subtracting the average spectral background and performing an interpolation to a linear k-space. The signal processing was performed on a 2.13 GHz dual core Intel® Xeon® based personal computer with 4GB DDRII SDRAM. The

Microsoft™ Windows XP® based application software was developed in C++ and made use of the Trolltech® QT v4.3 framework, the GNU Scientific Library v1.8 and the FFTW v3.1.2 library.

All figures display the logarithm of the squared signals, and are rescaled and adjusted to optimize contrast and brightness. The z-axis of the tomograms were rescaled by an estimated sample index of n=1.33 in order to represent geometrical distances rather than optical path lengths. Apart from the *in vivo* images, for which an image registration was performed, no post processing was applied. Figures 2(d) and 3(a) were produced using Voxx, a freeware 3D rendering program. The supplementary online videos 3 and 4 were rendered with Imaris® (Bitplane AG, Zürich, Switzerland).

Semi-automatic islet detection. In order to perform statistical analysis, the tomograms were screened for islet like structures. Determination of the islet volume and position was achieved by manually defining a region of interest and automatic extraction of the precise islet shape by filtering and thresholding (see electronic supplementary material). The obtained volumetric islet mask was used to estimate the mean of the islet signal. Likewise, the mean of the exocrine tissue surrounding the islet was extracted. The difference of these two values gives a measure of the contrast of an islet. In a further step, the signal variation within the islet core was analysed to evaluate homogeneity, expressed as the lateral gradient of the mean signal in function of depth within the islet, going from the outer surface to its inner core.

Preparation of dissected pancreas. All animal studies were approved by the Cantonal Veterinary Office (Vaud, Switzerland) and were conducted in accordance with the Swiss animal protection Law.

Pancreata (n=13) from three months old ICR female mice (Harlan Laboratories Ltd, Itingen, Switzerland) kept in normal housing and with food ad libidum (2018 Teklad Global 18% Protein Rodent Diet, Harlan Laboratories Ltd, Itingen, Switzerland) were dissected. The samples were fixed for 45 min in a 4% paraformaldehyde solution in PBS at room temperature, prior an overnight incubation in a 30% sucrose solution in PBS at 4°C. The samples were placed on a coverslip, on top of humidified filter paper, in order to avoid dehydration. Different regions were presented to the objective to obtain an overview of the pancreatic organ structures.

Immunohistochemistry. Three samples studied by xfOCM were embedded in Tissue-Tek OCT, frozen at -80°C and 8µm thick sections were prepared. Sections were washed in PBS and blocked with PBS and 10% Fetal Calf Serum (FCS) during 30 min at room temperature. Primary antibodies (Insulin 1:100, Linco, St. Charles, United States; DBA lectin 1:500, Vector Lab Inc, Peterborough, England; CD31/PECAM1 1:50, BD Biosciences, Allschwil, Switerzland) were diluted in PBS containing 10% FCS and 0.2% triton 100X (Tris HCL PBS Triton), and incubated with the sections overnight at 4°C. Sections were washed in PBS, incubated for 1 hour with secondary antibodies (Alexa 405, 488, 555, Invitrogen, Basel, Switzerland) diluted in TBST, washed in PBS and mounted. The sections were analysed on a

Leica DM 5500 with a 10X objective, using excitation wavelengths adapted to each fluorochrome.

Sample preparation from streptozotocin injected mice. C57B6 male mice were controlled for normoglycaemia and then injected once intraperitoneally (i.p.) with either 0.22 mg/g (w/w) of freshly prepared streptozotocin (Sigma Chemical Co, St Louis, MO, USA) or the corresponding volume (15 µl/g) of the 0.1 M citrate buffer (pH 4.5) which was used to dissolve the drug. Thereafter, blood glucose levels of all animals were evaluated every 3 days using a Glucocheck [22].

4-7 days after the streptozotocin injection animals were killed and the pancreata were rapidly sampled, weighed and cut into two fragments. One fragment was immediately extracted in 5 ml acid ethanol for evaluation of insulin content, as evaluated by a radioimmunoassay [22]. The other fragment was fixed for xfOCM under double blind conditions.

For xfOCM, the samples were mounted between a coverslip and sample holder, by means of a plastic spacer of 1mm thickness. For each sample, four regions of 1x1.5mm each were randomly chosen and scanned. The resulting tomogram stacks were then inspected to semi-automatically detect and classify the islets (Video 1, electronic supplementary material shows the overview of all measured samples).

***In vivo* experiment.** Adult ICR mice (n=5) (Harlan Laboratories Ltd, Itingen, Switzerland) were anesthetized with i.p. injection of a solution of 14.5 mg/kg Rompun® (Bayer AG, Switzerland) and 90 mg/kg kétasol® 100 (Dr. E.Greaub, Switzerland). The flank skin was shaved and cleaned with Betadine swab. An incision of 0.5-1 cm was made through the abdominal muscles to gently pull out the duodenum encircling the head of the pancreas. The duodenum was stabilized around a pillar during the scanning procedure. The mouse was exposed to a heating lamp and both pancreas and intestine sprayed with 0.9% NaCl during the modus operandi. Within 30 minutes from the beginning of the operation the measurement was completed and the incision sutured.

Statistical Analysis. Results are expressed as means ± SE. Differences in the mean values of blood glucose and insulin content were tested by analysis of variance, using the SPSS program (SPSS Inc., Chicago, IL, USA). For the difference in the means of islet contrast and homogeneity a t-test with unequal variances was performed.

RESULTS

***Ex vivo* imaging of pancreas.** To investigate the contrast and the structures which can be observed with xfOCM, we excised and fixed the whole pancreata of adult wild type mice and placed them on microscope slides. The optical setup was mounted on a table in the horizontal direction and the sample was accessed from the side, as indicated in figure 2 (a). The pancreas can be segmented into a tail (t) or splenic part attached to the spleen and a head (h) encircled by the duodenum, connected by a thin neck (n). Figure 2 (b) shows the tomogram of a B-scan of the neck of a pancreas. Two islets of Langerhans of different size are clearly visible as spherical structures with high contrast. The xfOCM signal arises from light

scattered by tissue discontinuities. The exocrine tissue has a more granular structure and scatters less light, whereas the ducts and vascular networks appear as dark regions with only their epithelial walls scattering incident light. Adjacent lateral scans were assembled to produce en face images (Fig. 2 (c)), and to generate 3D renderings of the whole volume data, allowing determination of the spatial position and the shape of the islets (Fig. 2 (d)). Supplementary videos 2 and 3 (electronic supplementary material) show en face scans at increasing depths and a 3D rendering respectively of the same volume data.

The semi-automatic islet detection helped to exploit this volumetric information and determine the amount of islets and their volume. Four regions of 1.5x1 mm each were scanned for three different animals. Figure 3 (a) depicts the total of 146 islets binned into different depth categories. Despite the scattering of the pancreatic tissue, which disturbs the propagation of the incident beam to deeper lying structures and ultimately limits the imaging depth, we could image islets up to more than 500 μm. The histogram of linearly increasing size categories (fig. 3 (b)) shows that many small islets were found, but only few of bigger size. The same data, but in a logarithmic scale is displayed in figure 3 (c). Islets down to a size of only about 15 μm in diameter (~2000 μm^3), corresponding to an aggregate of only a few cells, are reliably detected.

Figure 3 (d) presents an assembly of tomograms from islets of different sizes and depths, illustrating the resolving power of xfOCM.

Validation of xfOCM tomograms by immunohistochemistry. To ascertain that the spherical structures were indeed islets, we sectioned a subset of the samples. Figure 4 shows alignments between immunostained sections and virtual sections through an xfOCM stack. Cryosections were immunolabelled to identify beta cells (anti insulin antibody), ducts (anti DBA lectin antibody) and blood vessels (anti PECAM antibody). Overlays showed good correspondence between the cryo-sections and the virtual sections from the xfOCM data (Fig. 4). The few differences in the matching result from the distortions that tissues undergo during fixation and cryo-sectioning, and were compensated by a slight scaling of the xfOCM data. This demonstrates the advantage of imaging the tissue structure in fresh, unfixed tissue, where the native tissue morphology is revealed. This argument has also been stressed in the context of other *in vivo* imaging studies [23].

Imaging of streptozotocin injected mice. To determine whether xfOCM could detect changes in beta cell mass, we injected a group of mice (n=7) with streptozotocin, a drug which selectively kills insulin-producing cells [24]. A control group (n=6) was injected with the citrate buffer that served as the vehicle for the drug. Four to seven days after injection all control mice showed normal levels of blood glucose (8.6 ± 1 mmol/l, n=6) and total insulin content (58.8 ± 15.4 μg per pancreas, n=6) (Fig. 5 (a, f)). In contrast, the mice that had received streptozotocin showed markedly increased ($p<0.002$) blood glucose levels (25.47 ±3.27 mg/dl, n=7) and a significantly lower ($p<0.001$) total insulin content (25.9 ± 15.6 μg per pancreas, n=7) (Fig. 5 (a, f)).

The xfOCM analysis of the samples, carried out under double blind conditions, showed that some of the pancreata contained numerous islets whereas others contained significantly ($p<0.001$) fewer islets (Fig. 5(b). Opening of the codes revealed that all of the pancreata of the former type were from control mice with normal glucose homeostasis, whereas all the samples of the latter type suffered from hyperglyceamia due to streptozotocin-injection.

The few islets remaining after streptozotocin treatment were of various sizes without privileged volume category. (Fig. 5 (g)). The contrast as well as the islet homogeneity exhibit a significant difference in their means ($p<0.001$) with respect to the control islets (Fig. 5 (c, h)), taking only into account islets bigger than 1000 μm^3. Figure 5 (d, e, i, j) shows two selected islets of approximately same size and depth in the tissue, evidencing the difference in homogeneity of control and treated islets. These experiments demonstrate that xfOCM can detect beta cell loss and alterations in streptozotocin-treated animals.

Imaging of pancreas *in vivo*. Finally we scanned the head of the pancreas (h) *in vivo* after laparotomy of anesthetized mice. To increase the scanning speed, small regions of 256x256 pixels were scanned with low sampling in less than five seconds. The few remaining movement artefacts were corrected with an image registration algorithm [25]. After imaging, the incision was sutured allowing the mouse to recover.

An overview of samples measured *in vivo* is shown in figure 6. Deriving the islets' shape and position relative to ducts, blood vessels and pancreatic lobes is possible with the three dimensional data (fig 6 (d), and videos 4 and 5, electronic supplementary material). The semi-automatically detected islets were analysed and revealed a stronger absorption of tissue in the living organism, limiting the imaging depth to about 300 μm, as indicated in figure 6 (f).

DISCUSSION

In this study, we first characterized the imaging capacity of xfOCM by measuring fixed and excised pancreatic tissue. Comparison with histology confirmed that xfOCM can detect islets of all sizes and their association with ducts and blood vessels. Next, we found that xfOCM can discriminate between the islets of animals that had normal insulin content from the mice suffering from hyperglycaemia and decreased insulin content as a result of the beta cell death induced by streptozotocin. The data show that xfOCM can detect changes in the number of islets and in the contrast and homogeneity of the few residual islets that survive the cytotoxic effect of the drug. The following measurements on living mice showed that xfOCM can visualise pancreatic lobules, ducts, blood vessel networks, and islets of Langerhans *in vivo*.

OCT is a well established clinical technique in ophthalmology for retinal imaging and is gaining importance for minimal invasive imaging of other biological tissues. OCT has been reported in an earlier work to image fixed pancreatic tissue and detect islets [26]. However, only the high, near isotropic resolution of xfOCM in combination with the in-parallel depth extraction performing high speed imaging allows *in vivo* imaging and generates tomograms exhibiting high contrast. This contrast is generated by an intrinsic sample property without any exogenous labelling. Hence, individual islets were visualised in the living organism as

well as in fixed tissue. The exact nature of the strong scattering of the islets remains yet unclear. Whether it is the whole structure of the beta cell that strongly scatters the light, as pointed out by the streptozotocin experiments, or only the insulin containing vesicles within the beta cells has to be shown by further experiments.

A recently published work [27] shows a procedure for imaging the pancreas *in vivo* with two photon microscopy and involves gluing the pancreas between two glass plates. In contrast, once the pancreas is exposed, xfOCM works contact-free without immersion or cover slides and requires only slight stabilization of the sample to suppress the breathing motion of several millimetres. Repeated measurements should be feasible, given the same area of the pancreas can be identified consecutively. For such longitudinal studies, the access to the pancreas could be simplified by employing an endoscope or a glass window in the abdominal wall, making our method minimally invasive.

With the three dimensional volumetric data at hand, quantitative measurements of islet volume, shape and signal strength was possible in a semi-automatic way. This analysis enabled the detection of subtle islet alterations, and provided islet size distributions. The well known exponential distribution of islet sizes [e.g. 7] was not matched here, because only a limited amount of the whole islet population was assessed. However, judging on the smallest detected islets of only 15 μm in diameter, the resolution of xfOCM is one order of magnitude higher than that of OPT [7].

Furthermore, the quantitative analysis estimated the imaging depth, which was more limited in living than in fixed samples. The achieved depths are comparable to those reported for two photon microscopy. A trade-off between a light source in a longer wavelength region and the resulting reduced axial resolution could further optimize imaging performance. Even then, it is unlikely that xfOCM could measure the whole volume of the pancreas. Still, the surface volume of the pancreas is screened with unprecedented accuracy, offering new insight into this organ. Essentially, with xfOCM the islets are studied in their natural environment, and disease evolution and islet destiny can be evaluated. This is in contrast to the anterior eye chamber imaging platform [12] that is limited to the study of the engraftment process and graft function in an immunologically privileged engraftment site. Although without molecular specificity, xfOCM is able to measure islets in potentially any site accessible to the microscope, provided the islets contrast with the surrounding tissue. Also, xfOCM could be combined with two photon microscopy, to provide the scattering and fluorescence signal in parallel.

The newest generation of line cameras further increase the imaging speed of xfOCM and will enable the monitoring of islets in real time to study the response to stimuli or drug administration. This increased speed will also enhance OCT's capacity to perform Doppler flow measurements, a technique we and others have previously used in the eye [28, 29]. This principle could be adapted to reveal the pancreatic blood flow and provide additional functional parameters. xfOCM's sensitivity should prove useful to monitor changes in beta cell number – for instance during islet regeneration [30] or upon islet transplantation to visualise the islets and their vascularisation in the recipient environment. Analysing

dispersion and spectral absorption characteristics in the sample could add further functional contrast such as variations in metabolite concentrations [31, 32]. Eventually, xfOCM could help design new PET and MRI probes, that selectively label the pancreatic beta cells and that are most needed for the forthcoming clinical imaging of pancreatic islets by these techniques. Adding a contrast agent for xfOCM to prospective probes would enable the monitoring of their dynamics and specificity on a microscopic scale.

ACKNOWLEDGEMENTS

This research was funded by the Swiss National Fonds and an EU grant (SNF grant 205321-10974, EU FP7-222980). J.G. is funded by the Beta Cell Biology Consortium (Grant NIDDK U19 DK072495-02). P.M. is further supported by grants from the SNF (310000-122430) and the JDRF (1-2207-158). R.A.L is also funded by an EU grant (FP7-201880). We would like to thank William Pralong (Life Sciences, Ecole Polytechnique Fédérale de Lausanne) for valuable discussions, Gisele Ferrand (Life Sciences, Ecole Polytechnique Fédérale de Lausanne) for her veterinary expertise, Antonio Lopez (Laboratoire d'Optique Biomédicale, Ecole Polytechnique Fédérale de Lausanne) for his work on the figure preparation, and Erica Martin-Williams (Laboratoire d'Optique Biomédicale, Ecole Polytechnique Fédérale de Lausanne) for critical reviewing.

DUALITY OF INTEREST

The authors declare that there is no duality of interest associated with this manuscript.

REFERENCES

1. Souza F, Freeby M, Hultman K, et al. (2006) Current progress in non-invasive imaging of beta cell mass of the endocrine pancreas. Current Medicinal Chemistry 13: 2761-2773
2. Evgenov NV, Medarova Z, Dai GP, Bonner-Weir S, Moore A (2006) In vivo imaging of islet transplantation. Nat Med 12: 144-148
3. Tai JH, Foster P, Rosales A, et al. (2006) Imaging islets labeled with magnetic nanoparticles at 1.5 Tesla. Diabetes 55: 2931-2938
4. Kim SJ, Doudet DJ, Studenov AR, et al. (2006) Quantitative micro positron emission tomography (PET) imaging for the in vivo determination of pancreatic islet graft survival. Nat Med 12: 1423-1428
5. Holmberg D, Ahlgren U (2008) Imaging the pancreas: from ex vivo to non-invasive technology. Diabetologia 51: 2148-2154
6. Sharpe J, Ahlgren U, Perry P, et al. (2002) Optical projection tomography as a tool for 3D microscopy and gene expression studies. Science 296: 541-545
7. Alanentalo T, Asayesh A, Morrison H, et al. (2007) Tomographic molecular imaging and 3D quantification within adult mouse organs. Nat Methods 4: 31-33
8. Dodt HU, Leischner U, Schierloh A, et al. (2007) Ultramicroscopy: three-dimensional visualisation of neuronal networks in the whole mouse brain. Nat Methods 4: 331-336
9. Hermann M, Pirkebner D, Draxl A, Margreiter R, Hengster P (2005) "Real-time"

assessment of human islet preparations with confocal live cell imaging. Transplant Proc 37: 3409-3411
10. Boffa DJ, Waka J, Thomas D, et al. (2005) Measurement of apoptosis of intact human islets by confocal optical sectioning and stereologic analysis of YO-PRO-1-stained islets. Transplantation 79: 842-845
11. Takahashi N, Nemoto T, Kimura R, et al. (2002) Two-photon excitation imaging of pancreatic islets with various fluorescent probes. Diabetes 51: S25-S28
12. Speier S (2008) Noninvasive in vivo imaging of pancreatic islet cell biology. Nat Med 14: 574-578
13. Hitzenberger CK (1991) Optical Measurement of the Axial Eye Length by Laser Doppler Interferometry. Invest Ophthalmol Vis Sci 32: 616-624
14. Huang D, Swanson EA, Lin CP, et al. (1991) Optical Coherence Tomography. Science 254: 1178-1181
15. Leitgeb RA, Villiger M, Bachmann AH, Steinmann L, Lasser T (2006) Extended focus depth for Fourier domain optical coherence microscopy. Opt Lett 31: 2450-2452
16. Fercher AF, Hitzenberger CK, Kamp G, Elzaiat SY (1995) Measurement of Intraocular Distances by Backscattering Spectral Interferometry. Optics Communications 117: 43-48
17. Leitgeb R, Hitzenberger CK, Fercher AF (2003) Performance of Fourier domain vs. time domain optical coherence tomography. Opt Express 11: 889-894
18. Yun SH, Tearney GJ, Vakoc BJ, et al. (2006) Comprehensive volumetric optical microscopy in vivo. Nat Med 12: 1429-1433
19. Jenkins MW, Adler DC, Gargesha M, et al. (2007) Ultrahigh-speed optical coherence tomography imaging and visualisation of the embryonic avian heart using a buffered Fourier Domain Mode Locked laser. Opt Express 15: 6251-6267
20. Izatt JA, Hee MR, Owen GM, Swanson EA, Fujimoto JG (1994) Optical Coherence Microscopy in Scattering Media. Opt Lett 19: 590-592
21. Huang SW, Aguirre AD, Huber RA, Adler DC, Fujimoto JG (2007) Swept source optical coherence microscopy using a Fourier domain mode-locked laser. Opt Express 15: 6210-6217
22. Charollais A, Gjinovci A, Huarte J, et al. (2000) Junctional communication of pancreatic beta cells contributes to the control of insulin secretion and glucose tolerance. Journal of Clinical Investigation 106: 235-243
23. Vincent P, Maskos U, Charvet I, et al. (2006) Live imaging of neural structure and function by fibred fluorescence microscopy. Embo Reports 7: 1154-1161
24. Lenzen S (2008) The mechanisms of alloxan- and streptozotocin-induced diabetes. Diabetologia 51: 216-226
25. Thevenaz P, Ruttimann UE, Unser M (1998) A pyramid approach to subpixel registration based on intensity. Ieee Transactions on Image Processing 7: 27-41
26. Tearney GJ, Brezinski ME, Southern JF, Bouma BE, Boppart SA, Fujimoto JG (1998) Optical biopsy in human pancreatobiliary tissue using optical coherence tomography. Dig Dis Sci 43: 1193-1199
27. Marianne M. Martinic MGvH (2008) Real-time imaging of the pancreas during

development of diabetes. Immunol Rev 221: pp 200-213
28. Leitgeb RA, Schmetterer L, Drexler W, Fercher AF, Zawadzki RJ, Bajraszewski T (2003) Real-time assessment of retinal blood flow with ultrafast acquisition by color Doppler Fourier domain optical coherence tomography. Opt Express 11: 3116-3121
29. Bachmann AH, Villiger ML, Blatter C, Lasser T, Leitgeb RA (2007) Resonant Doppler flow imaging and optical vivisection of retinal blood vessels. Opt Express 15: 408-422
30. Moogk D, Hanley S, Ramunas J, et al. (2007) Design and analysis of a long-term live-cell imaging chamber for tracking cellular dynamics within cultured human islets of Langerhans. Biotechnol Bioeng 97: 1138-1147
31. Esenaliev RO, Larin KV, Larina IV, Motamedi M (2001) Noninvasive monitoring of glucose concentration with optical coherence tomography. Opt Lett 26: 992-994
32. Leitgeb R, Wojtkowski M, Kowalczyk A, Hitzenberger CK, Sticker M, Fercher AF (2000) Spectral measurement of absorption by spectroscopic frequency-domain optical coherence tomography. Opt Lett 25: 820-822

Figure Legends

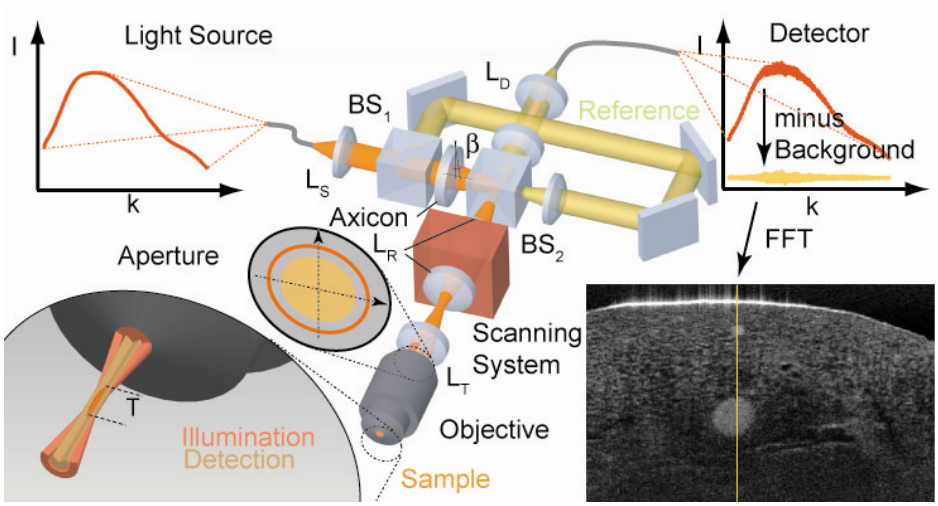

Figure 1: Principle layout of the xfOCM setup. The incoming broadband light is collimated (L_S) and split by beamsplitter BS_1 into sample and reference beam. The light in the sample arm passes through the axicon, is relayed by lenses L_R through the scanning system and focused by L_T into a thin annulus in the objective's aperture (small inlet). In the sample region, interference produces a light-needle which extends over a long axial range T (big inlet), scanning the sample in the lateral directions. The backscattered light is recombined with the light from the reference arm at beamsplitter BS_2 and coupled into the detection fibre by L_D. The detected interference pattern is corrected by the reference spectrum and Fourier transformed from the k-space to the axial coordinate of the sample structure.

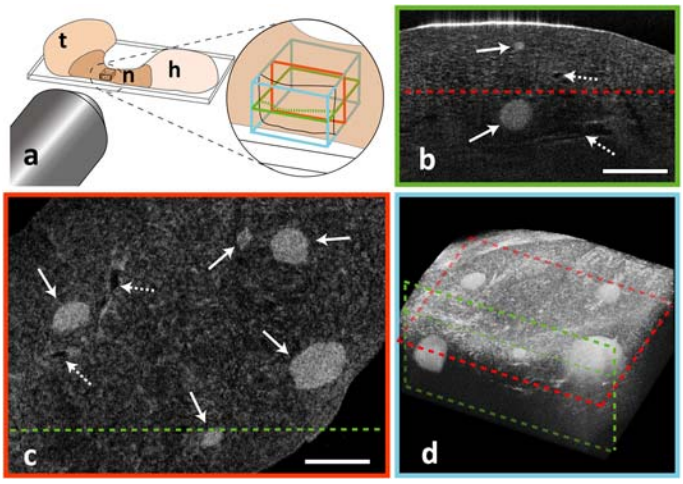

Figure 2: Scanning principle of xfOCM. (**a**) Scanning along one lateral direction creates a B-scan tomogram (green rectangle). Acquiring many B-scans by scanning along the second lateral direction provides a 3D volume (blue cube). En face images can be generated by selecting one depth (red rectangle). The pancreas consists of the head (h) and the tail (t), connected by the neck (n). (**b**) B-scan of a fixed sample, measured in the neck region depicting a 1 mm x 0.65 mm field (Scale bar: 250 µm). Two small islets are present (arrows), along with vessel-structures (dashed arrows). The bright line at the top of the tomogram indicates the sample surface that strongly reflects the incident light. (**c**) En face image at a depth of 220 µm showing 5 islets (arrows) and vessels (dashed arrows) (Scale bar: 250µm). (**d**) The volume data can be represented with a 3D rendering, giving a three dimensionsonal impression (1.5 x 1 x 0.65 mm). See also supplementary videos 1 and 2 for the complete volume data and a 3D rendering.

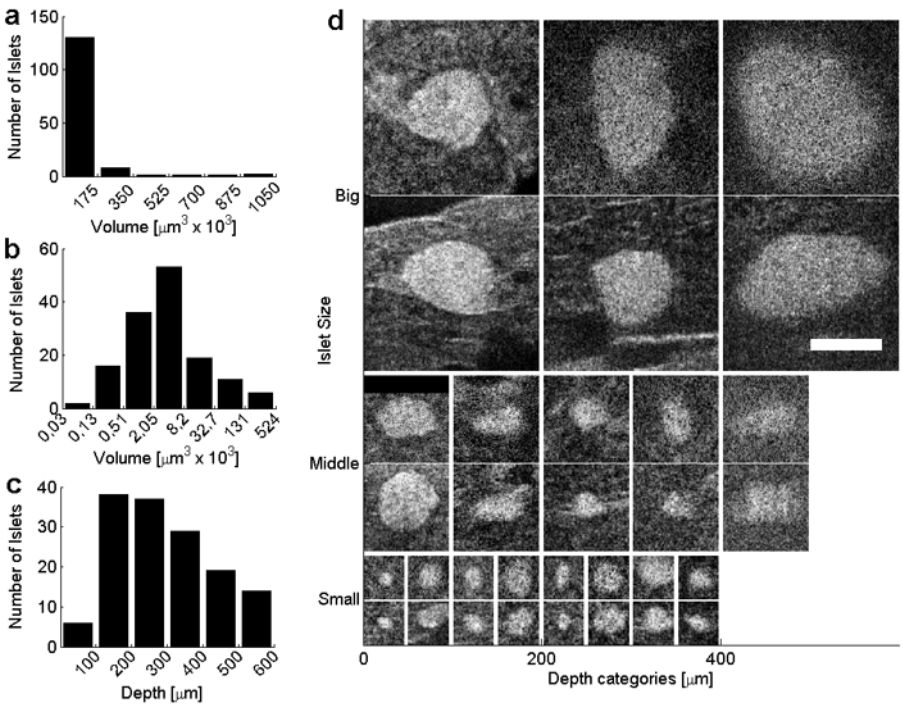

Figure 3: (**a)** Size distribution of the islets in linear scale (n=3, 3mm^3 per animal analysed).(**b)** The same data as in (a), but organised in logarithmic scale, where each size category is four times the volume of the previous one, demonstrates the resolving power of xfOCM. (**c)** Depth distribution of the detected islets. Close to the surface, the pancreas has less islets than in the deeper lying tissue. The reduced number of islets for bigger depths points out the detection limits of the method.
(d) Islets of different sizes and at different sample depths. Each islet is shown with a en face view (top) and a B-scan (bottom). The depth categories indicate that the islets were found within the first 200 µm, between 200 µm and 400 µm, and beyond 400 µm in the tissue, respectively. At increasing depth, the lateral resolution is blurred. Scale bar: 100 µm.

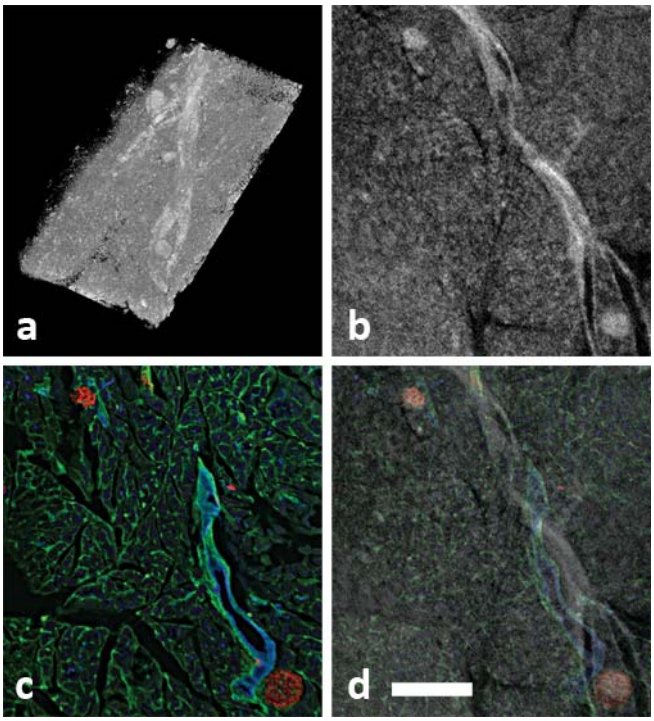

Figure 4: (**a**) 3D-rendered volume (0.86 x 1.7 x 0.78 mm) of the pancreas head. (**b**) Virtual section of the tomographic data. (**c**) Cryosection of the same area, immunohistochemically labelled for insulin (red), PECAM (green) and DBA lectin (blue). (**d**) Overlay of cryosection with xfOCM data identifying the islets and vessel structures (Scale bar 250 µm in **b**,**c** and **d**).

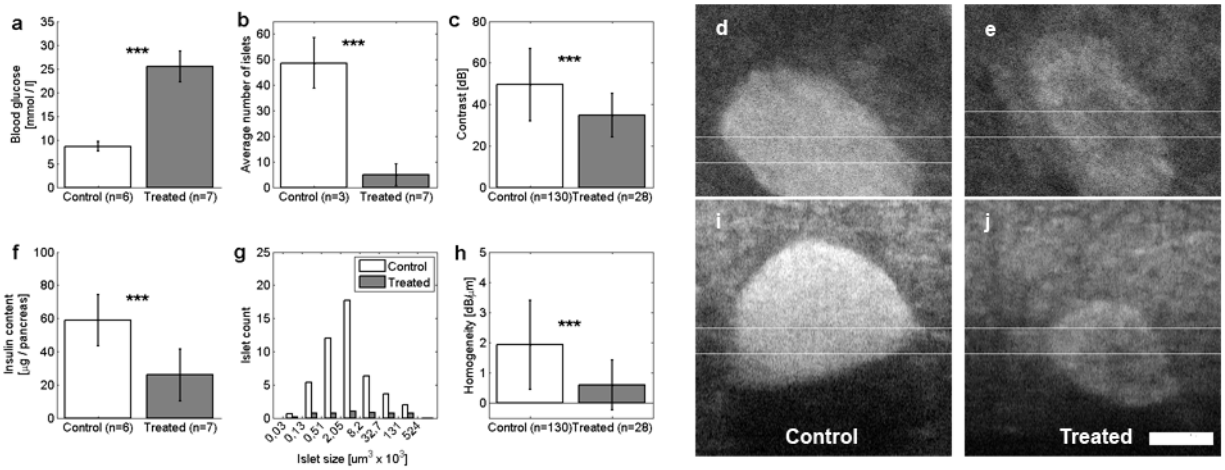

Figure 5: Exposure of C57B6 mice to streptozotocin (solid bars) resulted in a marked increase in blood glucose levels (**a**) and in a parallel decrease in the insulin content of the pancreas (**f**) compared to the control group (white bars). The selective beta cell death induced by the drug also decreased the number of islets found in the analysed regions of interest (**b**, screened tissue volume of 2.5mm^2 per animal). **g** The logarithmic distribution of the islet size exhibits a characteristic pattern for the control islets that is lost in the case of the remaining islets of treated animals. The few remaining islets (only islets >1000 µm^3 taken into account) likewise show a reduced contrast (**c**) and homogeneity (**h**). (a,b,c,f and h show means ± SE,***p<0.001).
An islet surviving in a diabetic mouse (**e**, **j**) shows a significant reduction in contrast, compared to a control islet (**d**, **i**). The columns show en-face (**d**, **e**) and B-scan (**i**, **j**) views, averaged over the 20 slides indicated by the white lines. The B-scans are adjusted in their axial position to show identical sample depths. The scale bar measures 100 µm and applies to all tomograms.

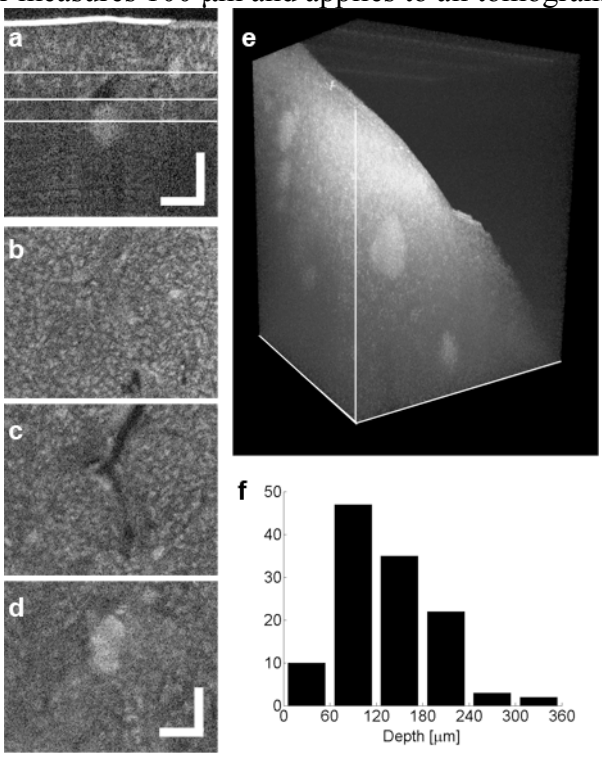

Figure 6: In vivo imaging of islets. (**a**) Side view and (**b,c,d**) corresponding en-face views (indicated by the white lines in the side view, median value over 5 slices) at different depths, showing islets and a

duct- or vessel-like structure. The scale bars measure 100 μm and apply to all views. (e) 3D rendering of a similar in vivo tomogram showing several islets at various depths, contained in a lobe of a pancreas. The volume measures 1mm x 1mm in the lateral directions and 500 μm in the vertical axis. (**f**) displays the depth distribution of the islets detected in vivo (6 animals, 123 islets).